Design and Experiment of Extended-range Power Supply System for Electric Tractor

Baochao Wang *, Yanshi Lv, Xianggang Chu, Dongwei Wang, Shuqi Shang

Posted Date: 30 July 2024

doi: 10.20944/preprints202407.2383.v1

Keywords: Electric tractor; Extended-range power supply; Double closed loop control; Droop control; Controlled rectifier

Article

Design and Experiment of Extended-range Power Supply System for Electric Tractor

Baochao Wang [1,*], Yanshi Lv [1], Xianggang Chu [2], Dongwei Wang [1] and Shuqi Shang [1]

[1] College of Mechanical and Electrical Engineering, Qingdao Agricultural University, Qingdao, 266109, China; lvyanshi7217@163.com(Y.L.); 200701031@qau.edu.cn(D.W.); sqshang@qau.edu.cn(S.S.)
[2] Weichai Lovol Intelligent Agricultural Technology CO., LTD, Weifang, 261200, China; chuxianggang@lovol.com(X.C.)
* Correspondence: wangbaochao@qau.edu.cn; Tel.: +86-131-3664-7120

Abstract: Electric tractors have many advantages, including high torque, excellent controllability, energy efficiency, simple structure, and electric interface for expansion. However, a significant limitation lies in their endurance. This study presents the design of an extended-range power supply system to ensure continuous endurance of electric tractor. The objective is to provide a continuous power source for our self-developed electric tractor while preserving the benefits of electric propulsion. Extended-range power systems utilize a primary mover, typically an oil-fueled internal combustion engine, to drive the generator for electricity generation, and the generated AC form electricity is subsequently converted into stable DC bus voltage by a power electronic converter. The hardware and control design of the extended-range power supply system have been finalized and validated through experimental trials. Results demonstrate the system's capability to sustain a stable DC bus voltage amidst disruptions such as sudden load shifts and fluctuations in prime mover speed. Even with 50% sudden load change, the voltage drop is within 12% and could recover to ±3% within 4 seconds. The range extender can be used alone without battery to power the electric tractor, or it can used in parallel with other extended-range extenders or battery thanks with the droop control ability for power sharing.

Keywords: electric tractor; extended-range power supply; double closed loop control; droop control; controlled rectifier

1. Introduction

Tractors represent the most prevalent type of machinery utilized in the agricultural production process [1,2]. Electric-powered tractors incorporate all the advantages of the electric drive, such as high power, simplified structure, easy expansion, good fuel economy, and low CO2 emissions compared to traditional pure diesel tractors [3–6]. It offer significant advantages especially in the regulation of distributed power systems and independent steering technology [7,8]. Nevertheless, the primary limitation of the device is the endurance time of the electric power supply [9–11].

A multitude of electric tractors have been developed utilizing disparate power supply techniques [12,13]. Since 2007, John Deere, Fendt, New Holland and other international agricultural equipment manufacturers have developed a number of electric tractor prototypes. In 2017, John Deere developed the SESAM, a battery-powered electric tractor that is capable of functioning for a maximum of only four hours at a medium load. In such designs, the battery typically occupies the majority of the vehicle's space. In 2018, John Deere developed a high-voltage cable-powered 400 hp electric tractor designated the GridCON, which eliminated the need for battery but requires high-voltage cable to power the tractor. In 2019, John Deere developed the 670 hp battery-and-cable-powered electric tractor "Joker" which contains only a small battery. In case of higher power output scenario, one or several "Joker" can be connected with " GridCON " to be powered by a high-voltage cable, and such group allows the cluster power to reach 1300hp [14,15], but the cable still remains a problem. Massey Ferguson proposed the concept of a 700 hp electric combine harvester, designated "Prototype 2030" which employs an extended-range electric power supply that utilizes oil as a fuel source to generate electricity. Extended-range electric tractors utilize a hybrid architecture that can reduce pollution on a small scale by utilizing the engine's highest fuel efficiency for power generation. This architecture is

 doi:10.20944/preprints202407.2383.v1

expected to have high research value and potential by 2030 [16,17]. Fendt has developed the 67 hp pure electric compact tractor, designated the "e100 Vario" which employs a pure battery-powered solution with 100kWh lithium-ion battery, but its continuous operation capability at medium load is only five hours. It is reported that the battery can be charged to 80% in 40 minutes with a CCS Type 2 plug [18]. In China, two prototype tractor were developed in collaboration between the National Agricultural Equipment Innovation Centre and the Luoyang Intelligent Agricultural Equipment Research Institute : a hydrogen fuel cell powered electric tractor named "ET504-H" and a 100 hp battery-changing prototype named "ET1004-W" [19–21]. In 2021, Qingdao Agricultural University developed a 15 hp extended-range electric crawler tractor named "Endeavor". The tractor is equipped with a double power supply, comprising a power battery and a range extender. The tractor is powered by the power battery during transportation and steering operations, while the range extender is activated during operations involving rotation and plowing, thus enhancing the vehicle's operational range [22–24].

In recent years, there are a lot of researches on hybrid vehicle energy management, such as Xiong proposes a new series-parallel electric bus energy management strategy, which is accomplished by two fuzzy logic controllers to complete the mode switching and power allocation [25]. Marzougui analyzes the energy management of hybrid power system of electric vehicle, and distributes the energy flow with the combination of multiple control algorithms [26]. Liu proposes the power supply and energy management strategy of electric tractor [27]. Li proposed a powertrain configuration and energy management strategy for electric vehicles that can save up to 30% energy [28]. Yu proposes a control strategy that employs fuzzy control rules and battery SOC to allocate motor torque based on demand torque [29].

The existing power supply methods can be broadly classified into five categories: pure battery, battery and supercapacitor, hydrogen fuel cell, cable power supply, and extended-range power supply [30,31]. Among these options, pure battery solutions are unable to meet the demand for high power and long range, while hydrogen and cable-powered solutions require significant infrastructure investment. The extended-range power supply enables the user to "use battery if available, burn oil to generate electricity if necessary" [32,33], thus eliminating the battery endurance problem. The extended-range power supply solution is a viable solution for powering electric tractors under current technical conditions [34–36]. However, the detailed design of a range extender system for tractor application has not been reported.

Accordingly, the objective of this paper is to give a detailed design of an extended-range power supply system to provide continuous electric power supply for electric tractors. The hardware design and control design have been completed and finally verified through bench experiments for both dynamic and steady-state performance.

2. Materials and Methods

2.1. Overall Design of the Extended-Range Power Supply System

This section presents the hardware design of the extended-range power supply system using DC bus, which was based on an analysis of the drive characteristics and power requirements of an independently developed electric tractor.

2.1.1. The Power Supply Architecture of the Extended-Range Electric Tractor

The electric drive system of an extended-range electric tractor is comprised of two primary parts: the power supply and the power consumption, as illustrated in Figure 1. The power supply encompasses the extended-range power system and the power battery. The power consumption encompasses the drive motor, electric hydraulics, electric PTO and transmission. The power supply and the power consumption are connected via a DC bus.

Unlike conventional range extender that works only by injecting current to the DC bus that with directly connected battery, in our study, the extended-range power supply system is designed to

 doi:10.20944/preprints202407.2383.v1

maintain a stable DC bus voltage, so that is can work alone or in parallel with other range extender or battery, providing more flexibility and possibility for power supply structure.

It comprises the prime mover, the generator, and the AC-DC converter. The prime mover rotates the generator, generating AC voltage. The AC-DC converter is responsible for transforming the AC voltage into a controlled DC voltage with a stable voltage. The control algorithm not only supports current control and voltage regulation, but also enables droop control, which is the decrease in output voltage as power increases. This could facilitate the parallel power sharing of multiple power source, thereby enabling the electric tractor to flexibly extend its overall power and energy capacity.

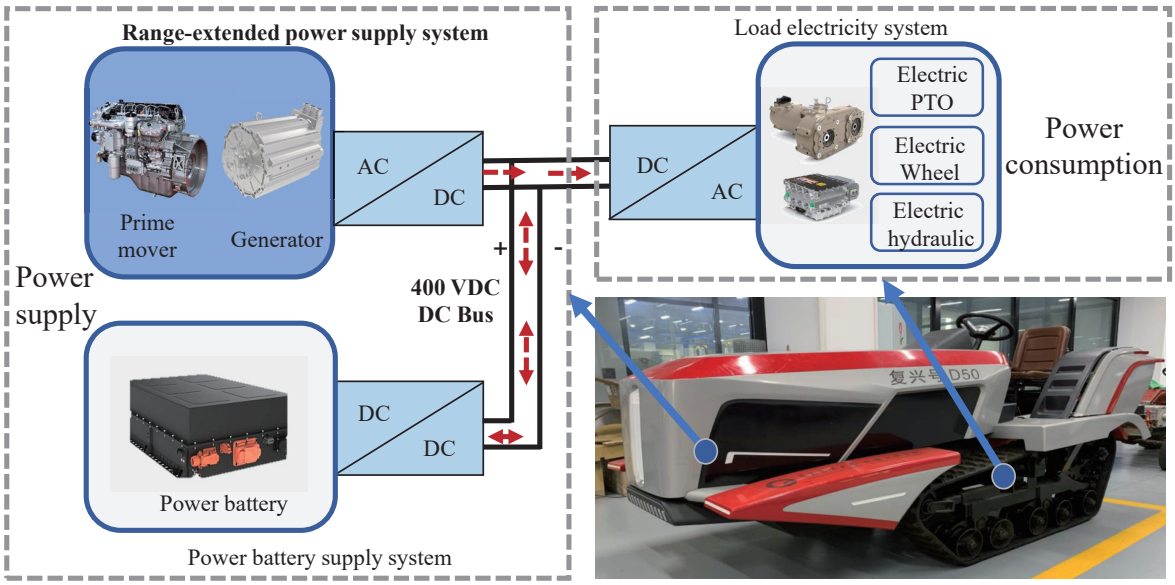

Figure 1. Power block diagram of the extended-range electric tractor system.

2.1.2. Hardware Design of the Extended-Range Power Supply System

1. Hardware Architecture

The interconnections of the components in the extended-range power supply system are illustrated in Figure 2. As previously stated, the prime mover is mechanically connected to the three-phase permanent magnet generator. The generator is electrically connected to a AC-DC converter. The output of the AC-DC converter is connected to the DC bus of the electric tractor.

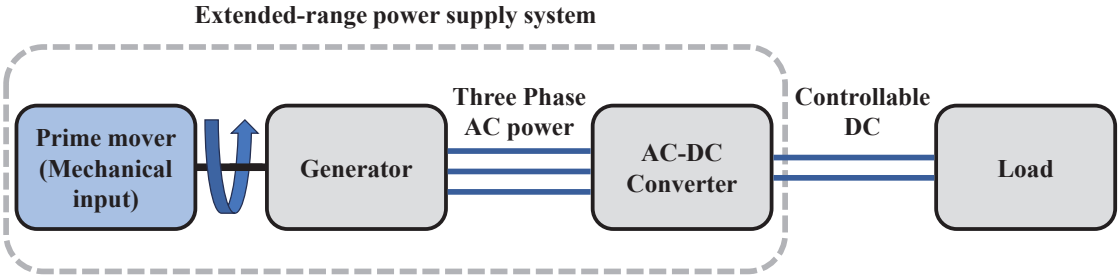

Figure 2. Power block diagram of the extended-range electric tractor system.

2. Determination of the DC Bus Voltage Level

It is important to consider the generator size and insulation voltage when determining the DC bus voltage. The generator size is selected using Equations (1) and (2).

$$D^2 l_{ef} = \frac{P'}{nC_A} \tag{1}$$

 doi:10.20944/preprints202407.2383.v1

$$P' = \sqrt{3}EI = T_e\Omega \tag{2}$$

where D is the motor armature diameter (m), l_{ef} is the length of the motor armature (m), P' is the motor -power (W), n is the rotation speed (r/min), C_A is a constant, E is the armature BEMF voltage (V), I is the motor armature current (A), T_e is the electromagnetic torque (N·m), Ω is the mechanical angular velocity (rad/s).

Equations (1) and (2) show that the size of the generator is proportional to the electromagnetic torque T_e, and the armature voltage E is proportional to the mechanical angular velocity Ω. Thus, for the same power, the higher the speed, the lower the motor torque, the smaller the size and the lower the cost. Therefore, when the power is at a certain level, the increasing of Ω should reduce the size, loss and cost of the motor. The increasing of Ω also increases E, and The DC bus should be greater than the line peak voltage of the motor. Taking into account the considerations mentioned above as well as the specifications of commercially available motors, a 400V DC bus voltage platform was chosen for the electric tractor.

3. Hardware Selection

Considering the operational requirements of the extended-range electric tractor, the principle should be satisfied that the battery serves as main the source and the range extender could supply concurrently or separately. In case of continuous heavy load, the battery and range extender could work together. The power should satisfy Equations (3),(4), and(5).

$$P_{bat} > P_T \tag{3}$$

$$P_{bat} + P_{RE} > P_{TMAX} \tag{4}$$

$$P_{RE} = kP_{bat} \tag{5}$$

where P_{bat} is the battery power (W), P_{RE} is the power of the extended-range power supply system (W), P_{TMAX} is the maximum power of the electric tractor (W), k is the design factor and k <1.

In this paper, the target power of the electric tractor is 20kW and the maximum power is 30kW. Equation (3) should be satisfied in pure electric mode. Equation (4) should be satisfied when the range extender and battery work together. As the power battery could provide 20kW, the required range extender is designed to be 10kW. According to the existing equipment, a 10.67kW prime mover and a 10kW generator are selected to make required range extender. The engine and generator are connected with belt, the connected transmission ratio is approximately 1.33. The final hardware configuration for the extender-range system is shown in Table 1.

Table 1. Electrical parameters of the extended-range power supply system.

Name	Parameters(Units)	Value
Generator	Rated power(kW)	10
	Rated current(A)	53.39
	Rated speed(r/min)	3000
	Frequency(Hz)	100
	Pole pair	2
	Armature resistance(ω)	0.07
	Armature inductance(mH)	0.84
Prime mover	Rated power(kW)	10.67
	Rated speed(r/min)	2200
AC-DC Converter	Rated voltage on the DC side(V)	400
	Rated current on the DC side(A)	25
	Switching frequency(kHz)	8
	Control functions	Current closed-loop control Voltage closed-loop control droop control

 doi:10.20944/preprints202407.2383.v1

2.2. Control Design of the Extended-Range Power Supply System

Three control algorithms are required to ensure power supply stability and quality: current control, voltage control, and droop control. This section elaborates on the design principles of the above three control algorithms.

Current and voltage control should have good dynamic and steady state performance. The current control should respond in milliseconds and the voltage control should respond in seconds to avoid large voltage drops. In addition, the droop control should achieve a proportional downward adjustment of the bus voltage as the output power increases.

2.2.1. General Overview of the Control Strategy of the Extended-Range Power Supply System

The control structure of the range-extender is shown in Figure 3. The prime mover rotates the generator to generate uncontrolled AC voltage, which is then transformed into controlled DC voltage, using FOC driving strategy with current control, voltage control and droop control.

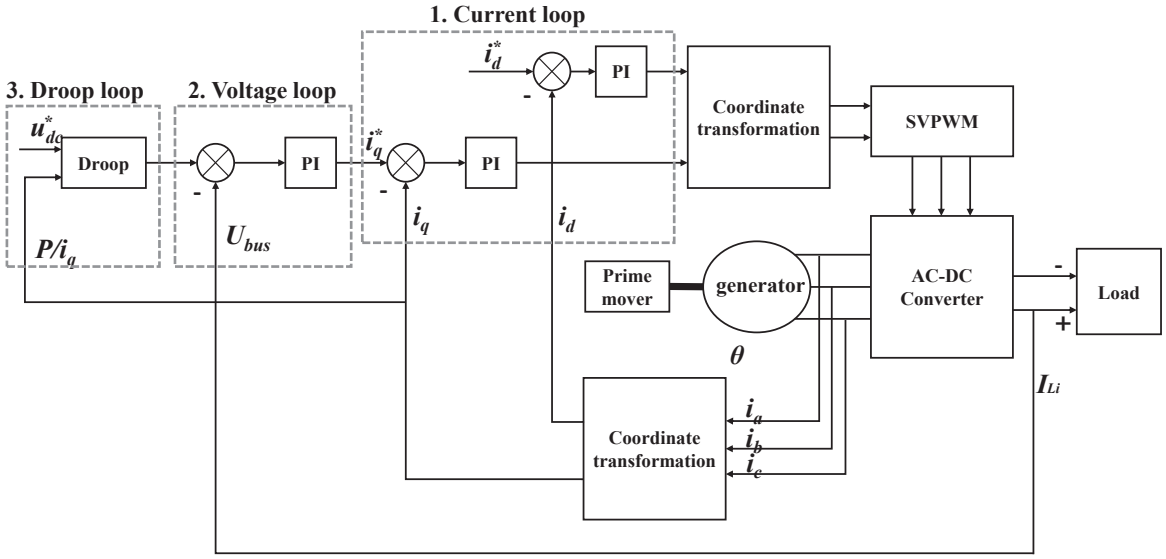

Figure 3. Block diagram of an extended-range power supply system.

In the control algorithm of Figure 3. i_a, i_b, and i_c are the three-phase stator currents (A), i_d and i_q are the d-axis current and q-axis current (A), i_d^* and i_q^* are the d-axis feed current and the q-axis current control reference (A), θ is the electrical angle of the generator(°), I_{Li} is the DC bus current (A), u_{dc}^* is a DC bus control voltage reference(V), P is the output power (W), U_{bus} is the actual DC bus voltage(V).

The current control first transforms the three-phase generator stator currents i_a, i_b, and i_c into i_d and i_q in d-q coordinate system by coordinate transformation. Then, the difference between i_d and i_q and i_d^* and i_q^* are then used as the error input to the current loop PI regulator to adjust the motor terminal voltage so that the current can be controlled to follow the given current reference. The voltage controller regulates the DC bus voltage by adjusting the q-axis current i_q through the voltage loop PI regulator. Droop control provides a downward adjustment of the DC bus voltage reference u_{dc}^* as output power increases, facilitating power sharing between multiple power supplies.

2.2.2. Mathematical Model of the Controlled Object of Extended-Range Power Supply System

The mathematical model of the generator model is necessary to develop the control strategy for extended-range power supply system. The generator used is a PMSM, and its model is given by Equation (6).

Preprints.org (www.preprints.org) | NOT PEER-REVIEWED | Posted: 30 July 2024 doi:10.20944/preprints202407.2383.v1

$$\begin{cases} U_d = R_s i_d + L_d \frac{di_d}{dt} - p\omega i_q L_q \\ U_q = R_s i_q + L_q \frac{di_q}{dt} + p\omega i_d L_d + \lambda p\omega \\ T_e = \frac{3}{2} p[\lambda i_q + (L_d - L_q) i_d i_q] \end{cases} \tag{6}$$

where U_d is the d-axis voltage (V), L_d is the d-axis inductance (H), U_q is the q-axis voltage (V), L_q is the q-axis inductance (H), p is the number of pole pairs of the motor; λ is the magnetic flux (Wb), ω is the rotor angular speed (rad/s), R_s is the stator resistance (Ω).

As mentioned above, the motor is driven by the FOC algorithm with i_d^* =0, and the model in Equation (6) can be simplified as in Equation (7), making the PMSM quite similar to a DC motor.

$$\begin{cases} U_d = R_q i_q + L_q \frac{di_q}{dt} + C_e \omega \\ T_e = \frac{3}{2} C_e i_q \end{cases} \tag{7}$$

where C_e is the back EMF coefficient, R_q is the armature resistance (Ω).

2.2.3. Design of Current Control for Extended-Range Power Supply System

Based on the plant in Equation (7), the current loop PI control block diagram is shown in Figure 4.

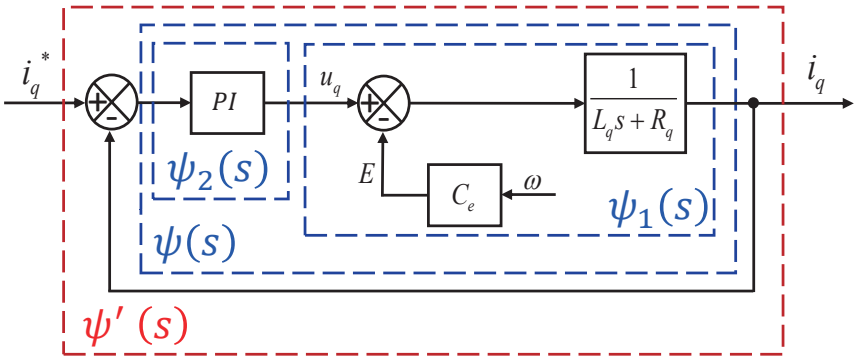

Figure 4. Current control equivalent structure diagram.

The transfer function of the plant for current control is noted as $\psi_1(s)$, and the PI controller transfer function is noted as $\psi_2(s)$, as given in Equations (8) and (9).

$$\psi_1(s) = \frac{1}{L_q s + R_q} \tag{8}$$

$$\psi_2(s) = \frac{K_{pi}(1 + T_{ii} s)}{T_{ii} s} \tag{9}$$

where K_{pi} is the proportional gain of the current controller; T_{ii} is the integration time constant of the current controller.

Therefore, the open loop transfer function $\psi(s)$ for current control can be represented by Equation (10).

$$\psi_(s) = \psi_1(s) \cdot \psi_2(s) = \frac{1}{L_q s + R_q} \cdot \frac{K_{pi}(1 + T_{ii} s)}{T_{ii} s} \tag{10}$$

According to $\psi(s)$, the open-loop Bode diagram can be plotted with different PI parameters, as shown in Figure 5.

In classical control theory, a larger area enclosed by the amplitude-frequency characteristic curve above the 0dB horizontal axis corresponds to a faster closed-loop response. Furthermore, a larger phase margin corresponds to a smaller closed-loop overshoot. Upon comparison of different parameters, it becomes evident that curve (a) not only ensures a sufficient enclosed area but also exhibits adequate

 doi:10.20944/preprints202407.2383.v1

phase margin and high-frequency suppression capability. In contrast, curve (b) displays a small enclosed area, signifying slower response. Meanwhile, curve (c) features a large enclosed area but lacks sufficient high-frequency attenuation capability with larger gain, rendering the closed-loop system susceptible to the influence of re-measurement noise and the discrete control effect curve. Consequently, the parameter K_{pi} =0.2, T_{ii} =0.015 are ultimately adopted from curve (a).

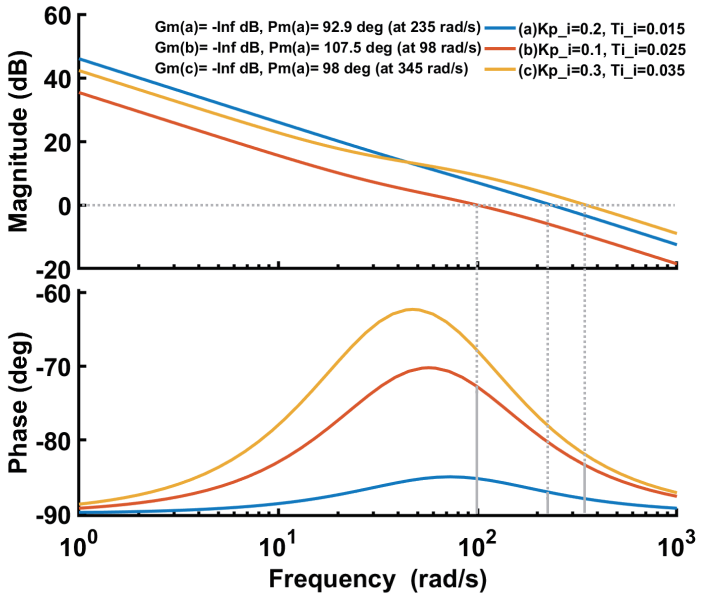

Figure 5. Open loop Bode diagram of current loop.

The closed-loop transfer function $\psi'(s)$ is given by Equation (11).

$$\psi'(s) = \frac{\psi(s)}{1+\psi(s)} = \frac{K_{pi}(1+T_{ii}s)}{T_{ii}s(L_q s + R_q) + K_{pi}(1+T_{ii}s)} \tag{11}$$

The closed-loop simulation is also carried out and the obtained closed-loop current control performance is shown in Figure 6. The settling time is approximately 20ms for a given 10A, which meets current control requirements of fast response.

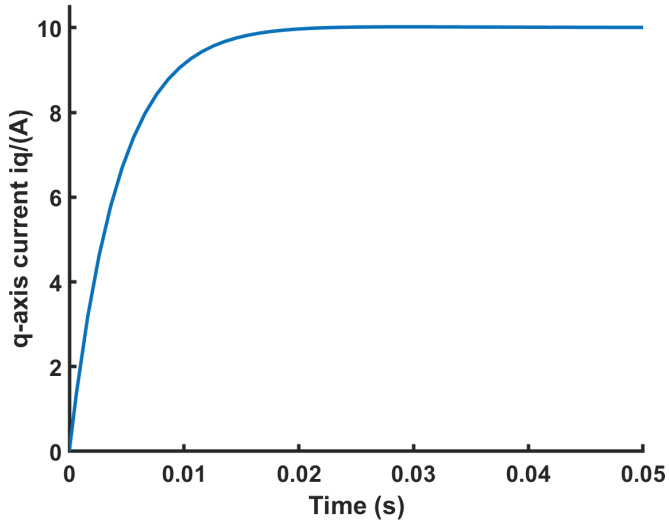

Figure 6. Response characteristics simulated curve of i_q.

 doi:10.20944/preprints202407.2383.v1

2.2.4. Design of Voltage Control for Extended-Range Power Supply System

For voltage control, the system includes the tuned current loop, the DC bus capacitor and the load. As the speed of the range-extender is essentially constant during steady state operation and the speed variation during dynamic adjustment was small, the influence of the rotational inertia and friction of the mechanical rotating parts can be ignored for the dynamic analysis. The voltage control block diagram can therefore be obtained as shown in Figure 7.

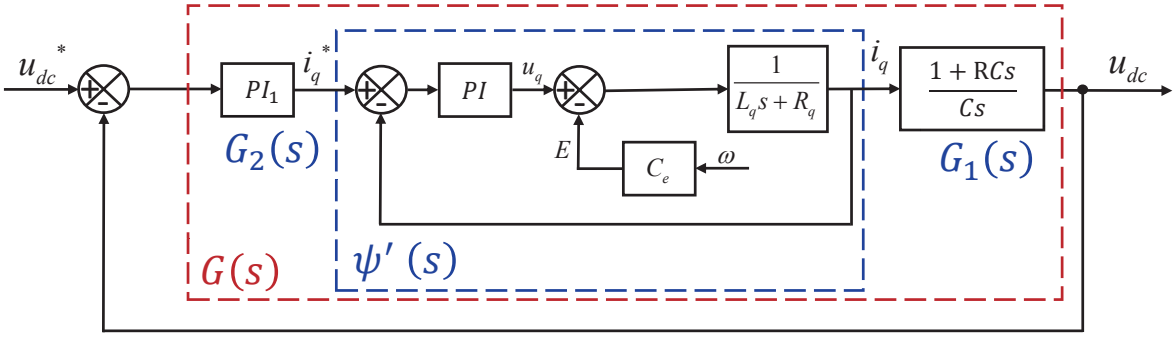

Figure 7. Equivalent structure diagram of voltage loop.

The DC bus transfer function $G_1(s)$ includes the capacitance C and the load R, and it is given by Equation (12).

$$G_1(s) = \frac{1 + RCs}{Cs} \tag{12}$$

where C is the voltage regulator capacitor (F), R is the load resistance (Ω).

The voltage controller is noted as $G_2(s)$, given by Equation (13).

$$G_2(s) = \frac{K_{pu}(1 + T_{iu}s)}{T_{iu}s} \tag{13}$$

where K_{pu} is the proportional gain of the voltage controller, and T_{iu} is the integral time constant of the voltage control.

The open-loop transfer function $G(s)$ for voltage control by is given by Equation (14).

$$G(s) = G_1(s) \cdot \psi'(s) \cdot G_2(s) \tag{14}$$

Similarly, the closed loop control performance with different control parameters is evaluated with open-loop bode diagram curve, as shown in Figure 8. The final selected control parameters are K_{pu} =0.01, T_{iu} =1.

Preprints.org (www.preprints.org) | NOT PEER-REVIEWED | Posted: 30 July 2024 doi:10.20944/preprints202407.2383.v1

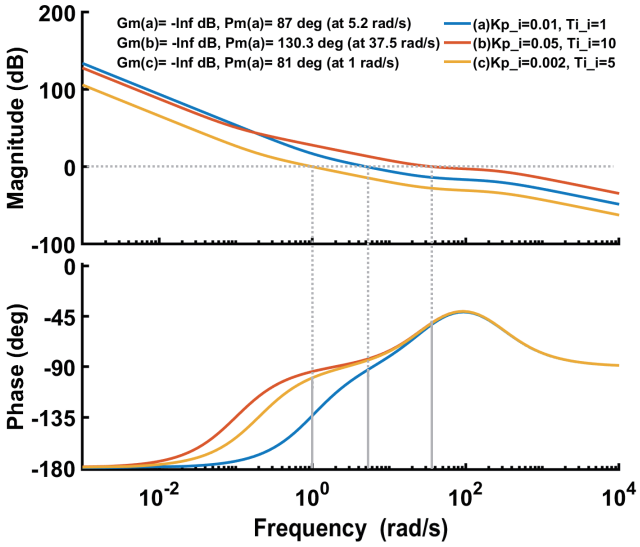

Figure 8. Equivalent structure diagram of voltage loop.

Then the closed-loop performance was verified. $G'(s)$ was closed-loop transfer function of the voltage loop, given by Equation (15).

$$G'(s) = \frac{G(s)}{1 + G(s)} \tag{15}$$

The closed-loop performance was evaluated by closed-loop simulation as shown in Figure 9. It can be seen that the DC bus voltage can be controlled at 400V. The voltage dropped by 48V when the 10kW load was suddenly added for 10s. After a response time of 3.5s, the 400V regulated voltage was recovered, and the overshoot of the recovery process was less than 1%. The dynamic response of the system was fast and smooth, with no steady-state errors, meeting the requirements of voltage control.

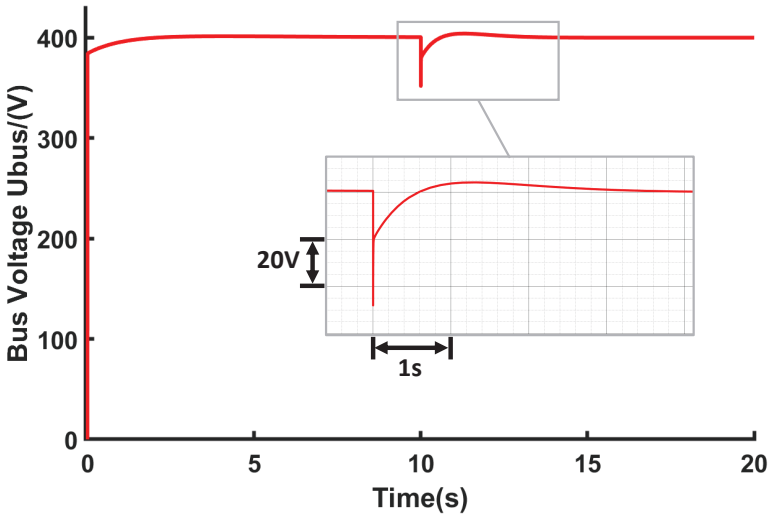

Figure 9. Simulation results of voltage control.

2.2.5. Design of Droop Control Parameters for Extended-Range Power Supply System

Droop control provides a downward adjustment of the DC bus voltage reference u_{dc}^* as output power increases, facilitating power sharing between multiple power supplies. The voltage droop control characteristic is shown in Figure 10. Principally, the droop control had a linear droop characteristic and the relationship between the DC bus voltage and current satisfied Equation (16).

 doi:10.20944/preprints202407.2383.v1

$$U_{bus} = u_{dc}^{*} - r_{di} I_{Li} \tag{16}$$

where r_{di} is the slope of the droop control.

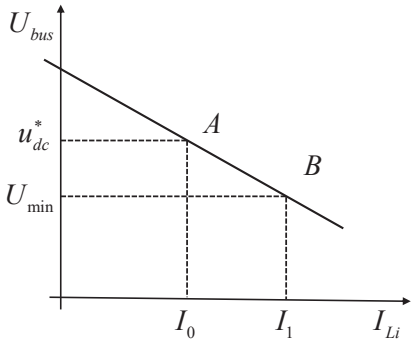

Figure 10. Characteristic curve of voltage droop control.

For droop control, the smaller the droop slope factor, the less the variation in the bus voltage, but the more difficult it is to share power between multiple sources. On the other hand, a large droop slope factor could reduce the efficient utilization of the DC bus voltage. In this application, the power generation class is 10kW, the maximum permissible bus voltage variation is 20V at rated generator power, the maximum DC bus current is 26A, finally the parameters are selected as r_{di} =0.77 according to Eq. (16).

3. Results and Discussion

This section provides the experimental verification of the designed extended-range power supply system. The control performance of the current loop, voltage loop and droop control are tested for steady state and dynamic performance, and the starting process is also optimized.

3.1. Experimental and Test Conditions

The extended-range power supply system experiment bench is shown in Figure 11. The extended-range power supply system experiment bench consists of a prime mover, generator, AC-DC converter and load. The load is simulated by a variable resistor.

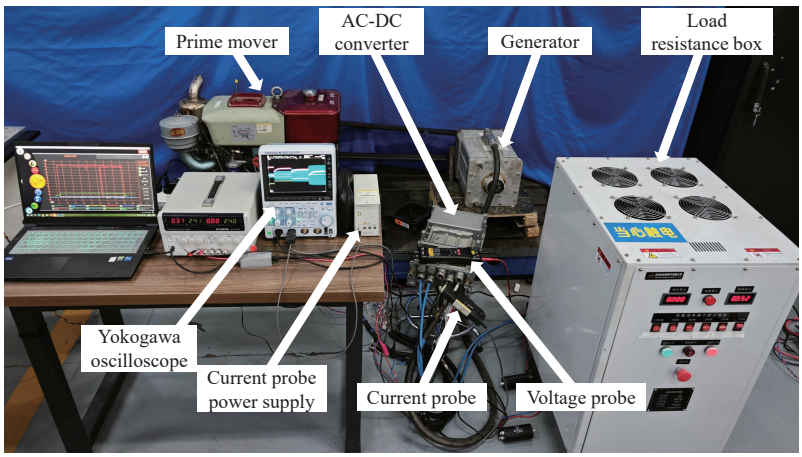

Figure 11. Extended-range power supply system experiment bench.

The load can be switched to different configurations under the tested voltage, corresponding to 1kW, 2kW, 5kW, 10kW power consumption, marked as Load 1 $\sim$ 4 respectively, and the resistance values are shown in Table 2.

 doi:10.20944/preprints202407.2383.v1

Table 2. Variable resistance load levels.

Load level name	Resistance value(Ω)	Corresponding power(kW)
Load1	160	1
Load2	80	2
Load3	32	5
Load4	16	10

Experimental data is collected by Yokogawa DLM3034 oscilloscope. High bandwidth probes are used to measure the bus voltage and the three-phase stator current of the generator.

3.2. Current Loop Control Characteristics Experiment

The dynamic and steady-state current control performance is verified. To avoid the influence of rotation, the dynamic performance is evaluated by locking the shaft and injecting current into the generator.

The current dynamic response obtained is shown in Figure 12(a). Ignoring the initial transient current burr due to start up injection for estimating generator position, it can be seen that for a given desired current of i_q^* =10A, the settling time is within 20ms, which is in consistence with the control design and simulation results. The steady state control performance is shown in Figure 12(b). The generator phase current waveform is stable and sinusoidal, indicating that good steady-state control performance.

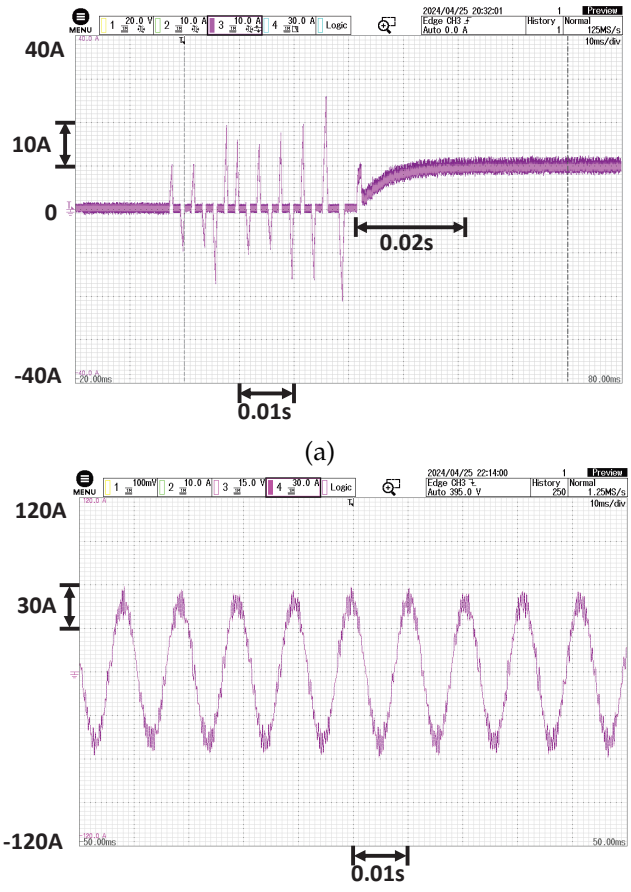

Figure 12. Bench experiment results of current control. (a) dynamic performance; (b) steady-state generator current waveform.

 doi:10.20944/preprints202407.2383.v1

3.3. Start-up Ramping

In the case of an extended-range power supply, there is a contradiction in the nature of the control parameters: the control parameter cannot be tuned either too fast or too slow. If the control parameter is too fast, it could cause an impact force on the prime mover during a sudden change condition, especially during the start-up, which may lead to the prime mover shutting down. If the control response is too slow, the DC bus voltage drop may be overly large in the condition of disturbance.

To handle this contradiction, this paper implements fast control parameters with a start-up ramp, and the ramp rate is set to 100V/s. The start-up process is tested at different speeds of 1400r/min, 1800r/min, 2200r/min, and 2600r/min, respectively, and the resulting bus voltage waveform is shown in Figure 13.

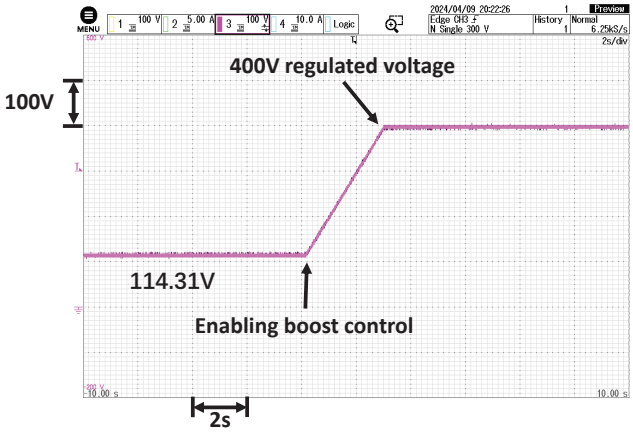

(a)

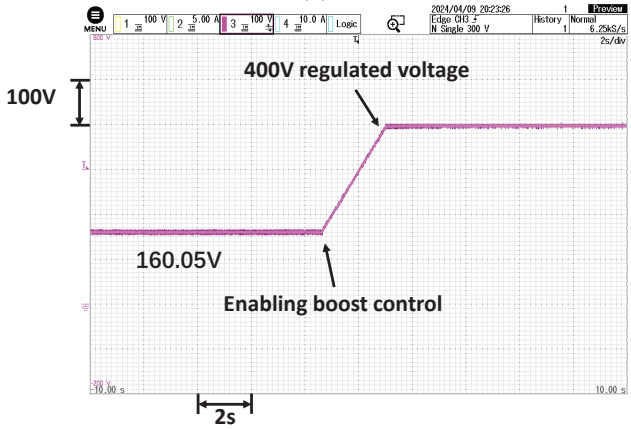

(c)

Figure 13. *Cont.*

 doi:10.20944/preprints202407.2383.v1

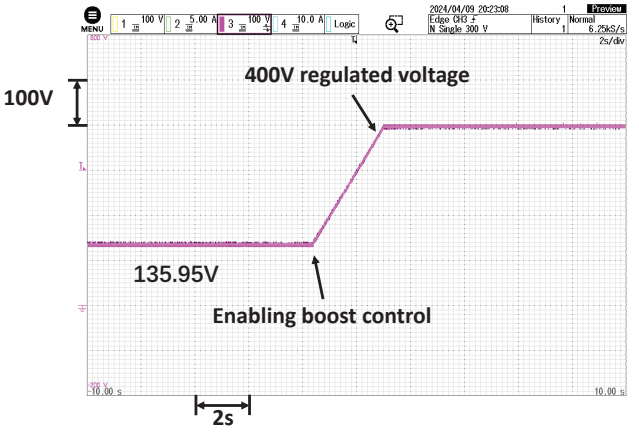

(b)

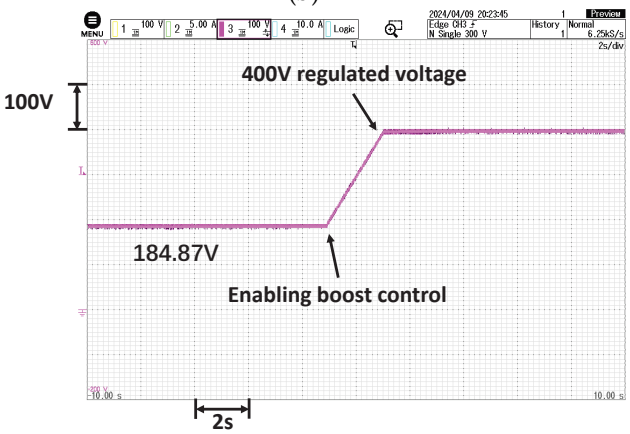

(d)

Figure 13. Starting procedure at different initial speed of prime mover. (a) 1400r/min; (b) 1800r/min; (c) 2200r/min; (d) 2600r/min.

With the start-up algorithm, the DC bus voltage could be ramped up smoothly from the unregulated voltage to the desired voltage with the desired ramp rate. The initial unregulated voltage comes from the inverter diode before the inverter chopping starts. The results show that the system can start at different speeds within 2s $\sim$ 3s to achieve 400V voltage stabilization, and the starting process is smooth and could avoid excessive impact to cause the prime mover shutdown.

3.4. Voltage Loop Dynamic Control Characteristics Experiment

The voltage control performance is evaluated experimentally, the dynamic performance is mainly focused because that the voltage control PI controller is able to ensure no steady-state error for voltage control.

The test is carried out in the following way: first the control is started to reach the steady state with stabilized voltage, then the load resistor is suddenly connected to the DC bus. The results of the DC bus voltage fluctuation and current waveforms are shown in Figure 14.

In Figure 14(a), (b), and (c), after the sudden introduction of 3kW, 5kW and 10kW loads, representing 30%, 50% and 100% loading, the DC bus voltage experiences reduction of 16V, 28V and 46V respectively. It is noteworthy that the maximum voltage drop remains within 12% of the rated voltage even with 100% sudden loading condition.

The maximum voltage recovery time under disturbance is less than 9s. The results show that the designed extended-range power supply system can ensure stable power supply to the load, even in case of 100% sudden load change.

 doi:10.20944/preprints202407.2383.v1

The DC bus current I_{Li} is shown in Figure 14(d). The DC bus currents step up to 7.48A, 12.83A and 22.58A respectively for different loads. There are no drastic fluctuations and overshoots in the load current. The transient process of voltage dip aligns with the current rise process following sudden load changes. Furthermore, the load current exhibits smooth behavior, demonstrating that the voltage control performance of the extended-range power supply system meets the design requirements.

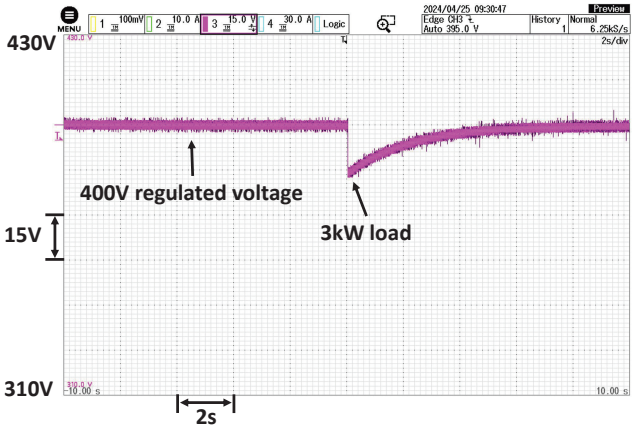

(a)

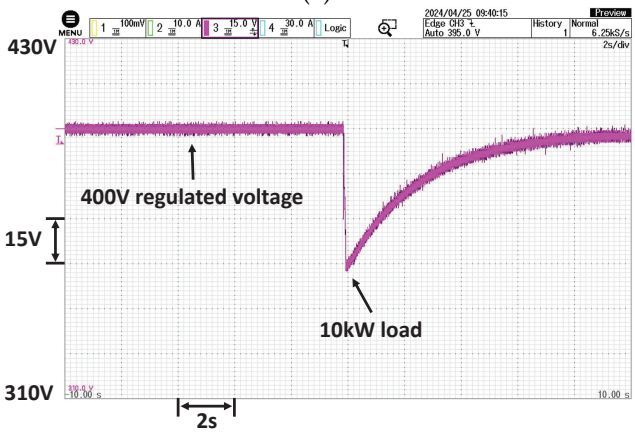

(c)

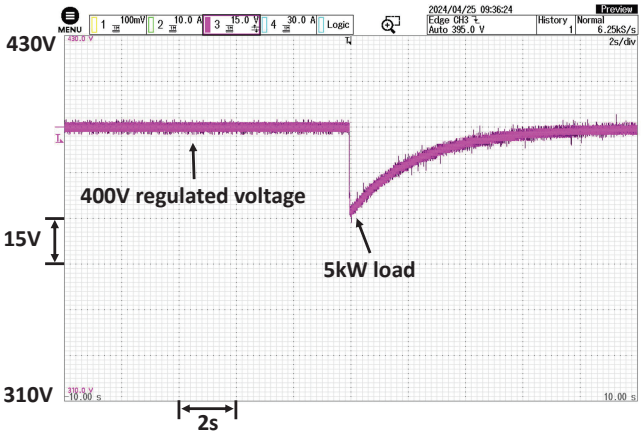

(b)

Figure 14. *Cont.*

 doi:10.20944/preprints202407.2383.v1

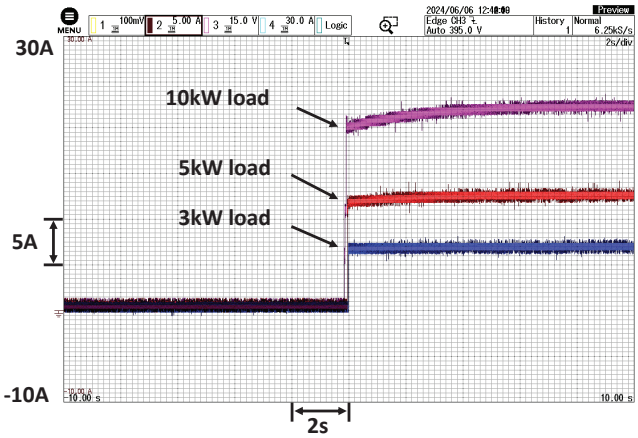

(d)

Figure 14. Bench experiment results of the voltage loop. (a) 3kW power loads; (b) 5kW power loads; (c) 10kW power loads; (d) DC current.

3.5. Droop Control Steady State Characteristics Experiment

Droop control facilitates the downward adjustment of the DC bus voltage with increasing output power, enabling power sharing among multiple sources without the need for intercommunication. The functionality of droop control is validated and tested across various load levels (0 kW, 3 kW, 5 kW and 10 kW), with r_{di} value set to 0.75. The resulting waveforms of the DC bus voltage and current are illustrated in Figure 15.

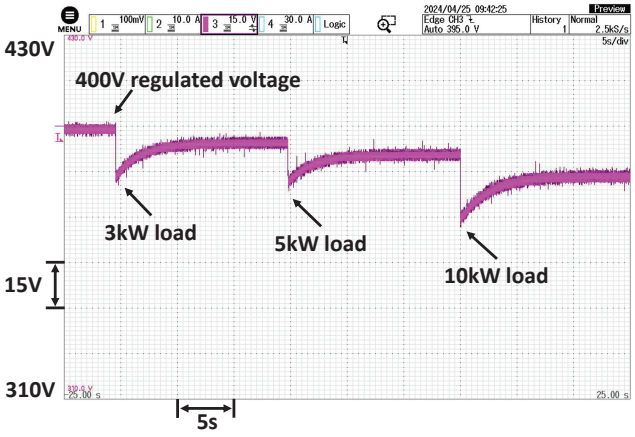

(a)

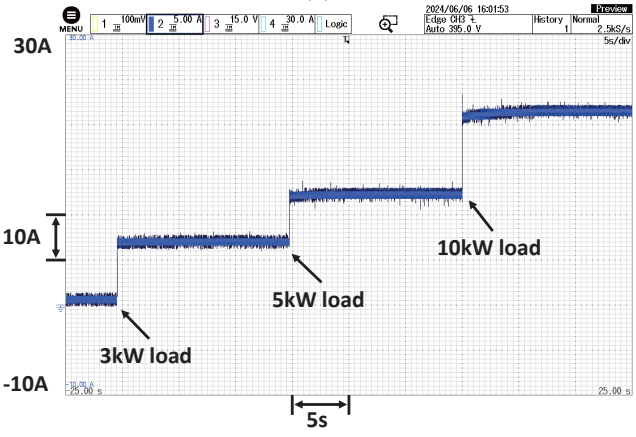

(b)

Figure 15. Bench experiment results of droop control. (a) bus voltage with varying load; (b) DC current.

 doi:10.20944/preprints202407.2383.v1

The DC bus voltage is shown in Figure 15(a). The DC bus voltage is initially stable at 400V. Then, when a 3kW load is switched on, the droop control eventually drops the voltage to 394.5V with a maximum 3% transient undershoot to 383.2V. For 5kW and 10kW loads, the corresponding final droop voltages are 390.8V and 383.2V, respectively, with maximum 2.6% and 3.5% transient undershoot to 380.5V and 369.8V.

In all cases the voltage transient undershoot could be recovered within 7s. The DC bus current I_{Li} is shown in Figure 15(b). The currents are 7.33A, 12.67A, and 22.37A for different loads. The calculated r_{di} values of the three different loads are 0.73, 0.75, and 0.74, respectively. The results are consistent with the control design and could meet the requirements.

4. Conclusions

In this paper, an extended-range power supply system has been designed with the aim of continuously powering our independently developed electric tractor. The hardware configuration and control design have been completed and experimentally tested for dynamic and steady-state operation.

The detailed design method and design process for the extended-range power supply system were given, including current control, voltage control and droop control. Experimental results showed that the actual performance is in accordance with the design requirement and simulation results. There is no steady state error for the DC bus voltage. In the transient test with sudden load change, the maximum DC bus voltage drop is less than 12%. The voltage droop recovers to within 3% range in less than 4s and the recovery time is less than 9s. The droop control works well with the design parameters, facilitating future power sharing between multiple sources without communication. The start-up process has also been optimized with ramp to avoid shutting down the prime mover. The designed system meets the requirements for continuous power supply of an electric tractor.

Author Contributions: Conceptualization, B.W. and Y.L.; methodology, B.W.; software, Y.L. and X.C.; validation, X.C. and Y.L.; formal analysis, Y.L.; investigation, B.W., X.C. and Y.L.; resources, B.W.; data curation, Y.L. and D.W.; writing—original draft preparation, Y.L.; writing—review and editing, B.W.; visualization, Y.L. and S.S.; supervision, D.W. and S.S.; project administration, B.W.; funding acquisition, B.W. All authors have read and agreed to the published version of the manuscript.

Funding: This paper was supported by the Collaborative Innovation Center for Shangdong's Main crop Production Equipment and Mechanization under Grant SDXTZX-22, Shandong Provincial Natural Science Foundation under Grant ZR2021ME018, National Key Research and Development Program of China under Grant 2022YFE0125800 and Lu-Yu Collaborative Project under Grant 2021LYXZ013.

Institutional Review Board Statement: Not applicable.

Data Availability Statement: The data will be made available upon reasonable request from the corresponding authors.

Acknowledgments: The authors would like to thank all those who contributed to this study.

Conflicts of Interest: The authors declare no conflict of interest.

Abbreviations

The following abbreviations are used in this manuscript:

SOC	State of Charge
BEMF	Back ElectroMotive Force
FOC	Field Orientation Control
PMSM	Permanent Magnet Synchronous Motor

References

1. Khatawkar, D.S.; James, P.S.; Dhalin, D. Modern trends in farm machinery-electric drives: A review. *Int. J. Curr. Microbiol. App. Sci* **2019**, *8*, 83–98.
2. Mileusnić, Z.; Petrović, D.; Đević, M. Comparison of tillage systems according to fuel consumption. *Energy* **2010**, *35*, 221–228.

 doi:10.20944/preprints202407.2383.v1

3. Janulevičius, A.; Juostas, A.; Pupinis, G. Tractor's engine performance and emission characteristics in the process of ploughing. *Energy Conversion and Management* **2013**, *75*, 498–508.
4. Katrašnik, T. Hybridization of powertrain and downsizing of IC engine–A way to reduce fuel consumption and pollutant emissions–Part 1. *Energy Conversion and Management* **2007**, *48*, 1411–1423.
5. Moreda, G.; Muñoz-García, M.; Barreiro, P. High voltage electrification of tractor and agricultural machinery–A review. *Energy Conversion and Management* **2016**, *115*, 117–131.
6. Moghadasi, S.; Long, Y.; Jiang, L.; Munshi, S.; McTaggart-Cowan, G.; Shahbakhti, M. Design and performance analysis of hybrid electric class 8 heavy-duty regional-haul trucks with a micro-pilot natural gas engine in real-world highway driving conditions. *Energy Conversion and Management* **2024**, *309*, 118451.
7. Deng, X.; Sun, H.; Lu, Z.; Cheng, Z.; An, Y.; Chen, H. Research on dynamic analysis and experimental study of the distributed drive electric tractor. *Agriculture* **2022**, *13*, 40.
8. An, Y.; Wang, L.; Deng, X.; Chen, H.; Lu, Z.; Wang, T. Research on Differential Steering Dynamics Control of Four-Wheel Independent Drive Electric Tractor. *Agriculture* **2023**, *13*, 1758.
9. Mao, Y.; Wu, Y.; Yan, X.; Liu, M.; Xu, L. Simulation and experimental research of electric tractor drive system based on Modelica. *Plos one* **2022**, *17*, e0276231.
10. Zhang, X.; Tan, S.C.; Li, G.; Li, J.; Feng, Z. Components sizing of hybrid energy systems via the optimization of power dispatch simulations. *Energy* **2013**, *52*, 165–172.
11. Wu, Z.; Wang, J.; Xing, Y.; Li, S.; Yi, J.; Zhao, C. Energy Management of Sowing Unit for Extended-Range Electric Tractor Based on Improved CD-CS Fuzzy Rules. *Agriculture* **2023**, *13*, 1303.
12. Faria, R.; Moura, P.; Delgado, J.; De Almeida, A.T. A sustainability assessment of electric vehicles as a personal mobility system. *Energy Conversion and Management* **2012**, *61*, 19–30.
13. Mousazadeh, H.; Keyhani, A.; Javadi, A.; Mobli, H.; Abrinia, K.; Sharifi, A. Life-cycle assessment of a Solar Assist Plug-in Hybrid electric Tractor (SAPHT) in comparison with a conventional tractor. *Energy conversion and Management* **2011**, *52*, 1700–1710.
14. Li, J.; Wu, X.; Zhang, X.; Song, Z.; Li, W. Design of distributed hybrid electric tractor based on axiomatic design and Extenics. *Advanced Engineering Informatics* **2022**, *54*, 101765.
15. Liu, M.; Lei, S.; Zhao, J.; Meng, Z.; Zhao, C.; Xu, L. Review of development process and research status of electric tractors. *Trans. Chin. Soc. Agric. Mach* **2022**, *53*, 348–364.
16. Flórez-Orrego, D.; Silva, J.A.; de Oliveira Jr, S. Exergy and environmental comparison of the end use of vehicle fuels: The Brazilian case. *Energy Conversion and Management* **2015**, *100*, 220–231.
17. Pali, H.S.; Kumar, N.; Alhassan, Y. Performance and emission characteristics of an agricultural diesel engine fueled with blends of Sal methyl esters and diesel. *Energy conversion and management* **2015**, *90*, 146–153.
18. Liu, M.; Li, Y.; Xu, L.; Wang, Y.; Zhao, J. General modeling and energy management optimization for the fuel cell electric tractor with mechanical shunt type. *Computers and Electronics in Agriculture* **2023**, *213*, 108178.
19. Li, X.; Xu, L.; Liu, M.; Yan, X.; Zhang, M. Research on torque cooperative control of distributed drive system for fuel cell electric tractor. *Computers and Electronics in Agriculture* **2024**, *219*, 108811.
20. Yang, H.; Sun, Y.; Xia, C.; Zhang, H. Research on energy management strategy of fuel cell electric tractor based on multi-algorithm fusion and optimization. *Energies* **2022**, *15*, 6389.
21. Chen, L.; Zhan, Q.; Wang, W.; Huang, X.; Zheng, Q. Design and experiment of electric drive system for pure electric tractor. *Transactions of the Chinese Society for Agricultural Machinery* **2018**, *49*, 388–94.
22. Wang, B.; Sechilariu, M.; Locment, F. Intelligent DC microgrid with smart grid communications: Control strategy consideration and design. *IEEE transactions on smart grid* **2012**, *3*, 2148–2156.
23. Wang, B.; Qiao, M.; Chu, X.; Shang, S.; Wang, D. Design and Experimental Study of Extended-Range Electric Caterpillar Tractor. *Trans. Chin. Soc. Agric. Mach* **2023**, *54*, 431–439.
24. Dong, Z.; Qin, J.; Hao, T.; Li, X.; Chi, K.T.; Lu, P. Distributed cooperative control of DC microgrid cluster with multiple voltage levels. *International Journal of Electrical Power & Energy Systems* **2024**, *159*, 109996.
25. Xiong, W.; Zhang, Y.; Yin, C. Optimal energy management for a series–parallel hybrid electric bus. *Energy conversion and management* **2009**, *50*, 1730–1738.
26. Marzougui, H.; Kadri, A.; Martin, J.P.; Amari, M.; Pierfederici, S.; Bacha, F. Implementation of energy management strategy of hybrid power source for electrical vehicle. *Energy Conversion and Management* **2019**, *195*, 830–843.
27. Liu, J.; Xia, C.; Jiang, D.; Sun, Y. Development and testing of the power transmission system of a crawler electric tractor for greenhouses. *Applied Engineering in Agriculture* **2020**, *36*, 797–805.

 doi:10.20944/preprints202407.2383.v1

28. Li, M.; Xu, H.; Li, W.; Liu, Y.; Li, F.; Hu, Y.; Liu, L. The structure and control method of hybrid power source for electric vehicle. *Energy* **2016**, *112*, 1273–1285.
29. Yu, Y.; Hao, S.; Guo, S.; Tang, Z.; Chen, S. Motor Torque Distribution Strategy for Different Tillage Modes of Agricultural Electric Tractors. *Agriculture* **2022**, *12*, 1373.
30. Alegria, E.; Brown, T.; Minear, E.; Lasseter, R.H. CERTS microgrid demonstration with large-scale energy storage and renewable generation. *IEEE Transactions on Smart Grid* **2013**, *5*, 937–943.
31. Justo, J.J.; Mwasilu, F.; Lee, J.; Jung, J.W. AC-microgrids versus DC-microgrids with distributed energy resources: A review. *Renewable and sustainable energy reviews* **2013**, *24*, 387–405.
32. Hou, X.; Zhang, X.; Huang, S.; Xu, P.; Shen, J. Measurement of engine performance and maps-based emission prediction of agricultural tractors under actual operating conditions. *Measurement* **2023**, *222*, 113637.
33. Ren, G.; Wang, J.; Chen, C.; Wang, H. A variable-voltage ultra-capacitor/battery hybrid power source for extended range electric vehicle. *Energy* **2021**, *231*, 120837.
34. Cao, X.; Han, M.; Nee, H.P.; Yan, W. A new method for simplifying complex DC systems and obtaining the controller droop coefficients. *IEEE Transactions on Power Systems* **2021**, *37*, 996–1006.
35. Ahmed, K.; Hussain, I.; Seyedmahmoudian, M.; Stojcevski, A.; Mekhilef, S. Voltage stability and power sharing control of distributed generation units in DC microgrids. *Energies* **2023**, *16*, 7038.
36. Lee, H.S.; Kim, J.S.; Park, Y.I.; Cha, S.W. Rule-based power distribution in the power train of a parallel hybrid tractor for fuel savings. *International Journal of Precision Engineering and Manufacturing-Green Technology* **2016**, *3*, 231–237.